




# Blue-LIRIC in the rabbit cornea: efficacy, tissue effects, and repetition rate scaling

RUITING HUANG,<sup>1,\*</sup> DAN YU,<sup>2</sup> DANIEL SAVAGE,<sup>1,3</sup> KAITLIN WOZNIAK,<sup>1,3</sup> LEN ZHELEZNYAK,<sup>4</sup> WAYNE H. KNOX,<sup>1,2,5</sup> AND KRYSTEL R. HUXLIN<sup>1,3,5</sup> 

<sup>1</sup>The Institute of Optics, University of Rochester, Rochester, NY 14627, USA

<sup>2</sup>Materials Science Program, University of Rochester, Rochester, NY 14627, USA

<sup>3</sup>Flaum Eye Institute, University of Rochester, Rochester, NY 14627, USA

<sup>4</sup>Clerio Vision, Inc., Rochester NY 14618, USA

<sup>5</sup>Center for Visual Science, University of Rochester, Rochester, NY 14627, USA

\*[rhuang9@ur.rochester.edu](mailto:rhuang9@ur.rochester.edu)

**Abstract:** Laser-induced refractive index change (LIRIC) is being developed as a non-invasive way to alter optical properties of transparent, ophthalmic materials including corneas *ex vivo* and *in vivo*. This study examined the optical and biological effects of blue-LIRIC (wavelengths 400–405 nm) of *ex-vivo* rabbit corneas. Following LIRIC treatment at low and high repetition rates (8.3 MHz and 80 MHz, respectively), we interferometrically measured optical phase change, obtained transmission electron microscopy (TEM) micrographs, and stained histological sections with collagen hybridizing peptides (CHP) to assess the structural and organizational changes caused by LIRIC at different repetition rates. Finally, we performed power and scan speed scaling experiments at three different repetition rates (1 MHz, 8.3 MHz, and 80 MHz) to study their impact on LIRIC efficacy. Histologic co-localization of CHP and LIRIC-generated green autofluorescence signals suggested that collagen denaturation had occurred in the laser-irradiated region. TEM imaging showed different ultrastructural modifications for low and high repetition rate writing, with discrete homogenization of collagen fibrils at 80 MHz, as opposed to contiguous homogenization at 8.3 MHz. Overall, this study confirmed that LIRIC efficacy can be dramatically increased, while still avoiding tissue ablation, by lowering the repetition rate from 80 MHz to 8.3 MHz. Modeling suggests that this is due to a higher, single-pulse, energy density deposition at given laser powers during 8.3 MHz LIRIC.

© 2022 Optica Publishing Group under the terms of the [Optica Open Access Publishing Agreement](#)

## 1. Introduction

Over the past two decades, ablative laser refractive surgeries, including photorefractive keratectomy (PRK), laser *in-situ* keratomileusis (LASIK), laser thermal keratoplasty (LTK), small incision lenticule extraction (SMILE) etc., have emerged as common approaches to correct ocular refractive errors. In femtosecond laser-assisted LASIK (femto-LASIK), femtosecond laser pulses are used to create a planar corneal flap. Ultraviolet light at 193 nm emitted by an excimer laser is then used to perform corneal stromal photoablation [1–4]. Modification of ocular refractive power is thus achieved by altering the curvature of the corneal surface via tissue removal. However, the inherently invasive nature of tissue ablation associated with traditional laser refractive procedures can result in post-surgical complications such as discomfort, dry eye, stromal haze, ectasia and deterioration of optical quality [5–12].

In an attempt to minimize these potential side effects, our group developed a novel, less-invasive, non-ablative technique for vision correction [13–18]. This technique uses tightly focused femtosecond laser pulses, with energies below the threshold for large-scale disruption of corneal tissue, to induce localized refractive index (RI) change in cornea. We refer to this technique as Laser-Induced Refractive Index Change (LIRIC). As early as 2008, Ding *et al.*

successfully inscribed periodic gratings in the stromal layer of post-mortem cat corneal tissue using a high repetition rate, near infrared (NIR), femtosecond pulsed laser; the induced RI change was estimated to be +0.008 by measuring the diffraction efficiency of the inscribed LIRIC pattern [19]. However, the scan speed was too slow (0.7  $\mu\text{m/s}$ ), making the procedure unacceptable for clinical applications. To enable clinical relevance at higher scan speeds, several enhancements to LIRIC have been investigated, such as employing shorter laser wavelengths at 400 nm or 405 nm or doping the cornea with biocompatible, multi-photon sensitizers [14,20–22].

Here, we should note that when discussing optical correctors, it is more accurate to describe, and measure induced optical phase change rather than RI change. Optical phase change,  $\Delta\phi$ , being directly proportional to RI change ( $\Delta n$ ), is defined in Eq. (1),

$$\Delta\phi = \frac{\Delta n \cdot L}{\lambda_{\text{measure}}} \quad (1)$$

where  $L$  is the axial thickness of the phase structure along the light's propagation direction, and  $\lambda_{\text{measure}}$  is the wavelength of the light used during the measurement. In this work, we set one wave of phase change and half a wave of phase change (@ 550 nm) as our benchmarks for fabricating different phase structures. It is worth noting that the 1 wave of phase change is critical for creating Fresnel lenses [16,17,23], while 0.5 waves of phase change is the target for the maximum phase shift of a presbyopia-correcting multifocal LIRIC wavefront [24,25].

The magnitude of LIRIC-induced phase change depends on material properties and writing parameters, both of which have been extensively studied in hydrogel-based polymers [26–30]. Here, we characterize the effects of Blue-LIRIC, defined as LIRIC treatment with 400–405 nm laser wavelengths, in *ex vivo* rabbit corneas and detail its impact on the corneal extracellular matrix (ECM) at the microscopic, chemical, and ultrastructural levels. We then correlated the tissue effects with regards to optical phase change at various repetition rates, average powers, and scan speeds. Our ultimate goal was to determine the optimal writing conditions to maximize optical phase change while minimize tissue disruption. Critically, in contrast to previous studies [14], we now show that it is possible to generate up to 1.0 waves of phase change at 550 nm in *ex vivo* rabbit corneas using a single LIRIC layer written at 405 nm, 200 mW and a scan speed of 100 mm/s by shifting from a high repetition rate to a lower repetition rate regime. Finally, our experimental results were contrasted with predictions from a proposed photochemical model [26,27], confirming likely mechanisms underlying observed tissue effects.

## 2. Methods

### 2.1. Laser writing parameters and protocols

To study the optical and biological impact of LIRIC in live cornea, laser processing experiments were carried out in freshly enucleated New Zealand White rabbit globes (purchased from Sierra for Medical Science, Whittier, CA, USA). Extracted rabbit eyeballs were immediately preserved in Optisol-GS (Bausch & Lomb, Inc., Rochester, New York), maintained at 4 °C, and shipped to our laboratory overnight on ice. On the day of arrival, they were kept refrigerated in Optisol-GS, and experiments were performed within two days.

Calibration phase bars (Fig. 1(a)) were written into the corneal stroma of each globe and consisted of a grid of rectangular regions (0.4 mm x 6 mm), with each rectangle written using constant laser parameters (e.g., power, scan speed, etc.), creating a piston wavefront. The piston wavefronts were written using raster scanning with 0.5  $\mu\text{m}$  line spacing. Previous studies have shown that 0.5  $\mu\text{m}$  line spacing creates a region of constant phase change rather than a phase grating with the writing and laser parameters used in these experiments [28]. We wrote the same LIRIC pattern and measured phase changes in different eyeballs ( $n \geq 3$ ). Fourteen excised rabbit globes were used in the power and scan speed scaling experiments. Four rabbit eyes were used for histological and ultrastructural analyses.

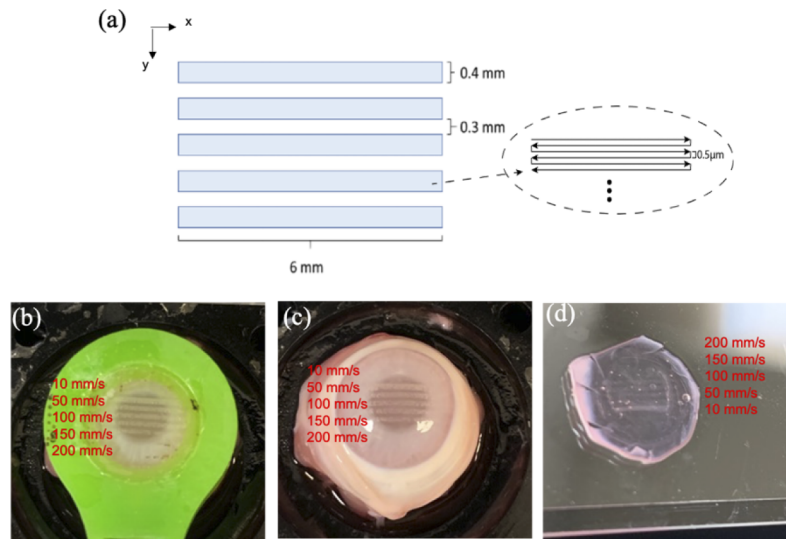


**Fig. 1.** (a) Schematic of LIRIC-induced phase bars. Each rectangular region was written with a fixed set of parameters. Phase bars were  $0.4 \times 6$  mm with a 0.3 mm inter-bar spacing. Each phase bar consists of 800 grating lines with a line spacing of  $0.5 \mu\text{m}$ , created by raster scanning the laser focal spot through the corneal tissue. (b-d) Photos of a rabbit eye globe with five LIRIC phase bars, created at scan speeds of 10 mm/s, 50 mm/s, 100 mm/s, 150 mm/s and 200 mm/s. Phase bars can be seen immediately after writing and with the applanator on top of the eye globe (b); immediately after writing and without the applanator (c); radial cut excised corneal tissue imaged two hours after immersing the written globe in Optisol-GS and refrigeration (d).

All Blue-LIRIC laser writing in this study was carried out using lasers with 400–405 nm central wavelengths. During LIRIC treatment, each LIRIC laser system interfaced to the ocular tissue with a flat applanation patient interface. The applanator (Fig. 1(b)) consisted of a custom-designed suction ring and a 1.0 mm thick planar glass window. The laser systems (Table 1) consisted of a femtosecond laser focused within the corneal stroma, as previously described [26,27,31,32]. For all test conditions, the pulse width was approximately 190 fs (Table 1).

To cover a broad range of repetition rates (1.0, 8.3, and 80 MHz), 3 laser systems were used. Specifications of each system are listed in Table 1.

Power scaling phase bars were written in a single LIRIC layer parallel to the epithelium and with a targeted depth of  $170 \mu\text{m}$  below the anterior corneal surface, corresponding approximately to the mid-stroma [see Fig. 2(c)]. Note that the epithelium was not removed for this procedure – LIRIC can be performed through an intact epithelium.

At 1.0 MHz repetition rate, average power ranged from 10 to 28 mW. Three layers with a  $20 \mu\text{m}$  layer spacing (center-to-center) were inscribed to improve the signal to noise ratio. The phase change per layer was obtained by dividing the measured phase change by the number of layers, 3, assuming that the phase shift is linear with the number of layers in the small signal region. At 8.3 MHz repetition rate, average power ranged from 50 to 200 mW. At 80 MHz repetition rate, average power ranged from 150 to 300 mW. For repetition rates of 1 and 8.3 MHz, the scan speed was 200 mm/s with a numerical aperture (NA) of 0.45 (system #1), corresponding to a diffraction-limited spot size of  $0.4 \mu\text{m}$  after taking into account the beam waist in the case of two-photon absorption. For the 80 MHz repetition rate system, the scan speed was 220 mm/s with a numerical aperture of 0.57 (system #2), resulting in a diffraction-limited spot size of  $0.32 \mu\text{m}$ . All spot size calculations assume a Gaussian beam profile. See Table 1 for details.

**Table 1. Specifications of laser writing systems used in the present study**

	System #1			System #2	System #3
<b>Laser</b>	KM Labs Y-Fi HP NOPA-SHG			Ti:Sapphire	Ti:Sapphire
<b>Repetition Rate</b>	1.0 MHz	8.3 MHz	8.3 MHz	80 MHz	80 MHz
<b>Scan Speed</b>	200 mm/s		10,50,100,150, 200 mm/s	220 mm/s	10,50,100 mm/s
<b>Average Power</b>	10–28 mW	50–200 mW	200 mW	150–300 mW	64 mW
<b>Single Pulse Energy</b>	10–28 nJ	6–24 nJ	24 nJ	1.88–3.75 nJ	0.8 nJ
<b>Pulse Width</b>	190 fs		190 fs	165 fs	100 fs
<b>NA</b>	0.45		0.45	0.57	0.4
<b>Diffraction Limited Spot Size</b>	0.4 $\mu\text{m}$		0.4 $\mu\text{m}$	0.32 $\mu\text{m}$	0.456 $\mu\text{m}$
<b># of Layers</b>	3	1	1	1	5
<b>Function</b>	Power Scaling	Power Scaling & Histology	Scan Speed Scaling	Power Scaling	Scan Speed Scaling & Histology

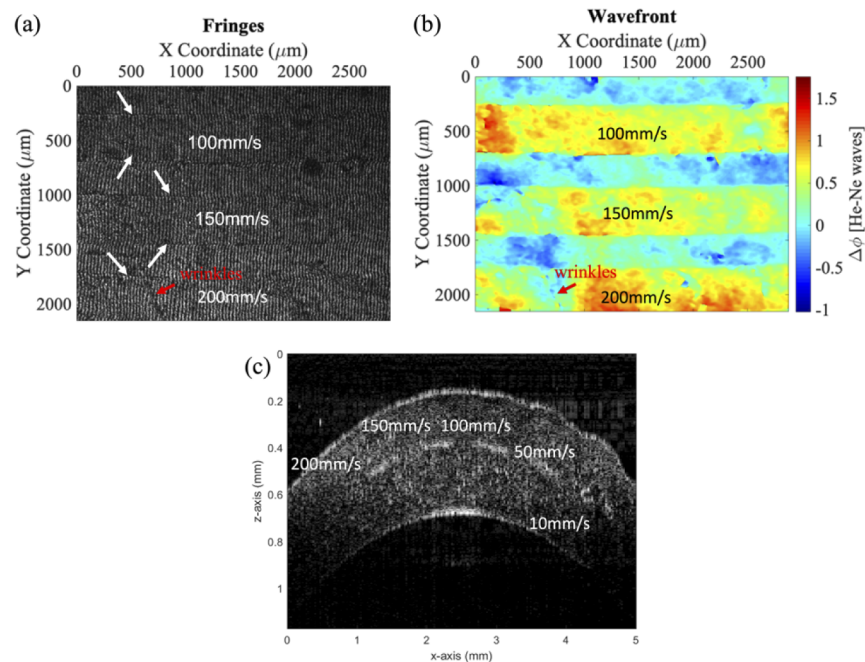


**Fig. 2.** (a) Interferogram, (b) wavefront image correspond to three phase bars created at 100 mm/s, 150 mm/s and 200 mm/s. White arrows mark the edges of phase bars and non-uniformity of the wavefront is caused by imperfect tissue quality (e.g., wrinkles), (c) OCT image of a written rabbit eye globe with five phase bars created at 10 mm/s, 50 mm/s, 100 mm/s, 150 mm/s and 200 mm/s (from right to left) Note severe damage in the 10 mm/s bar.

LIRIC's dependence on scan speed was assessed from 10 to 200 mm/s with a constant average power of 200 mW in a single layer at 8.3 MHz (system #1). Scan speed scaling experiments were also performed at 80 MHz on system #3 with a much lower average power of 64 mW (due to a maximum power limitation of the laser), a NA of 0.4 (corresponding to a diffraction-limited spot size of 0.456  $\mu\text{m}$ ) and a pulse duration of 100 fs. Due to the limited maximum power of system #3, we had to write 5 layers to induce measurable photo-modification in corneal tissue. Additionally, system #1 and system #3 were implemented to perform histological analysis at 8.3 MHz and 80 MHz.

Photos of a written rabbit eyeball with and without the applanator are shown in Fig. 1(b-d). Phase bars could be clearly seen immediately after writing due to the presence of microbubbles, which subsequently dissipated (Fig. 1(d)). The cause of microbubbles is still a matter of speculation, but our hypothesis is that a small amount of gas was briefly generated because of the combination of heat accumulation and thermoelastic tensile stress, as demonstrated by Vogel *et al.* [33].

The sclera is discolored pink in Fig. 1(d) largely because the Optisol solution has a pink color to it. As the eyes were extracted and then transported in this solution (something that lasted at least 24 hours), and since it took us some time to cut out the cornea, perform LIRIC (with the cornea and attached sclera in an Optisol solution) before imaging, this gave the Optisol time to absorb into the tissue, and color the white sclera pink.

## 2.2. Post-LIRIC tissue processing

After LIRIC, globes were bisected along the retinal equator. Internal structures (crystalline lens, iris, and vitreous humor) were removed, leaving the cornea with a 4–8 mm scleral ring. The cornea and surrounding sclera were then mounted on to a customized wet cell and held in place by an annular scleral clamp. The wet cell submerged the cornea in Optisol-GS and was walled by optical windows, as described previously [17,34]. The wet cell was then placed in the sample arm of a custom-built Mach-Zehnder Interferometer (MZI) to perform optical phase change measurements.

## 2.3. Optical phase change measurements

Optical phase change induced by LIRIC were measured with an MZI, consisting of a helium neon laser (632.8 nm wavelength) and an imaging sensor capturing the interference pattern formed by the reference and sample arm of the MZI [23,35]. In the sample arm of the MZI, a dissected cornea, mounted in the custom wet cell described above and submerged in Optisol-GS was placed in a plane optically conjugate to the imaging sensor. There was no untreated cornea in the reference arm. The induced phase change was the difference between the optical path length inside the LIRIC-treated region and the optical path length inside the laser-untreated region, as previously described in our publications [23,24]. The optical phase change (i.e., LIRIC-induced wavefront) was calculated from the interferogram (Fig. 2(a)) using a carrier fringe algorithm [23,36,37]. The wavefront was subsequently unwrapped at 550 nm (instead of 632.8 nm) to match the peak sensitivity of the human eye, and the background wavefront was subtracted after fitting to Zernike polynomials. A phase map example corresponding to an interferogram consisting of phase bars written at 8.3 MHz is shown in Fig. 2(b). Optical coherence tomography (OCT) imaging was performed to visualize the position of LIRIC patterns inside the corneas, as shown in Fig. 2(c). The axial thickness of the LIRIC patterns was measured to be approximately 20  $\mu\text{m}$ . One thing to note is that in the case of multiple layer writing, layer separation was set to be 20  $\mu\text{m}$  (center-to-center) by the axial translation stage. Therefore, when layers themselves were 20  $\mu\text{m}$  thick, as in higher-energy-deposition cases (Fig. 2(c)), the LIRIC-free gap between two adjacent layers was 0  $\mu\text{m}$ ; if layers were thinner than 20  $\mu\text{m}$  as in lower-energy-deposition cases (e.g. the 80 MHz patterns), then the LIRIC-free gap would be greater than 0  $\mu\text{m}$ . Corneal



tissue was severely damaged at the slowest scan speed of 10 mm/s at 8.3 MHz, and as a result, the phase change attained could not be measured.

#### 2.4. Tissue processing for electron microscopy and histology

Four *ex vivo* New Zealand White rabbit eyes were used for histological and ultrastructural analyses. The powers used were 200 mW at 8.3 MHz, and 64 mW at 80 MHz. Immediately after LIRIC, each rabbit cornea was dissected and bisected, with one half processed for TEM and the other half for histological analysis. No TEM micrographs and histological images were captured at 1 MHz. Because the phase change induced at 1 MHz was smaller than that at 80 MHz, this made the patterns difficult to visualize in the fresh corneas. After fixation, they became invisible, making it impossible to dissect them accurately for TEM and histological processing. As such, they were not included in the present TEM imaging.

Processing for TEM: Immediately after performing Blue-LIRIC, the region of the cornea containing the inscribed phase gratings was excised and processed for TEM. The excised tissue was immersion-fixed in 0.1 M sodium cacodylate buffered 4% paraformaldehyde + 2.5% glutaraldehyde for 2–4 hours. It was then rinsed and post-fixed for 60 minutes in 1.0% osmium tetroxide. Finally, the tissue was rinsed in distilled water, dehydrated through a graded series of ethanol to 100%, transitioned into propylene oxide, and infiltrated with EPON/Araldite epoxy resin overnight. The corneal tissue was embedded into fresh resin in a mold and polymerized at 65 °C for 48 hours. Epoxy sections 1  $\mu\text{m}$  thick were cut and stained with toluidine blue to identify the inscribed LIRIC pattern, which was then thin-sectioned using a diamond knife. The sections were then placed onto formvar/carbon nickel ( $2 \times 1 \text{ mm}^2$ ) slot grids. The grids were stained with aqueous uranyl acetate and lead citrate and examined with a Hitachi 7650 TEM and photographed with an attached Gatan Erlangshen 11-megapixel digital camera system.

Processing for histology: Excised cornea were immersion fixed in 1% paraformaldehyde/0.1 M Phosphate Buffered Saline (PBS; pH 7.4) for 10 minutes and then transferred into 30% sucrose in 0.1 M PBS at 4 °C for 48 hours. The tissue was embedded in Tissue Tek O.C.T. Compound (Sakura Finetek, CA), frozen, transversely sectioned into 20  $\mu\text{m}$ -thick slices using a cryostat (2800 Frigocut E, Reichert-Jung, Depew, NY), and mounted onto gelatin-coated microscope slides. Sections were stored at –20 °C until staining. Sections containing the LIRIC pattern were easily identified by their characteristic green auto-fluorescence under 488 nm microscope illumination (Olympus, AX70) [38]. They were reacted with 2  $\mu\text{M}$  (1:50) biotin-collagen hybridizing peptide (B-CHP, 3Helix Inc., UT) in 0.1M PBS, and incubated overnight at 4 °C; 1 section per slide was incubated in PBS only to serve as a negative staining control. CHPs bind specifically to globally unfolded collagen strands; this is primarily thought to occur when collagen is denatured [39–41]. Following overnight incubation, the sections were washed, and Streptavidin Alexa Fluor 555 conjugate (Invitrogen, NY) diluted in PBS and 5% normal horse serum was applied for 1 hour, in the dark, at room temperature. After a final rinse in PBS, slides were cover-slipped with mounting medium containing DAPI (Vector Laboratories, CA), which labels all live cell nuclei in each section.

#### 2.5. Photochemical model

We recently developed a photochemical model based on a nonlinear, multiphoton absorption mechanism and an overwriting factor [26,27,42,43]. This model was intended to illustrate the effects of various laser system parameters on the magnitude of the induced phase change under different laser exposure conditions. As briefly mentioned above in the context of microbubble generation, we posit that LIRIC likely induced both a photochemical and a thermal reaction in the tissue. Our motivation for suggesting that the photochemical effect dominated the reaction, causing refractive index/phase changes, is based on prior work by our group [14,22]. In that work, we reported our findings showing that the efficacy of LIRIC could be enhanced either by

using a shorter laser wavelength or by applying a photosensitizer to improve the two-photon absorption (TPA) coefficient of corneal tissue.

In brief, considering a pulse train incident on the focal plane, the induced phase change was assumed to be proportional to the amount of pulse energy deposited at the same site, represented as single pulse energy multiplied by an overwriting factor assuming a linear accumulation. The overwriting factor,  $N$ , caused by a two-dimensional pulse overlapping effect can be given by the following equation, assuming a top-hat pulse intensity distribution,

$$N = \frac{2\omega \cdot \nu}{S} \cdot \frac{2\omega}{t} \quad (2)$$

where  $\omega$  is the beam size after being focused by a microscope objective,  $\nu$  is the laser repetition rate,  $S$  is the scan speed, and  $t$  is the line spacing. To correlate the induced phase change with the total amount of energy deposition, we assumed the deposited pulse energy could be absorbed by the material via a nonlinear, multiphoton absorption process. In the case of 405 nm LIRIC in corneal stroma, a two-photon absorption process was expected as the cornea is transparent at 405 nm and has a strong absorption in the ultraviolet. The transmittance of the corneal tissue was measured by a spectrometer, and the results are shown in Huang *et al* [42].

Detailed mathematical derivation can be found in our previous work [26,27,42,43]. The final version of a photochemical model, in the case of a two-photon absorption process, can be expressed in terms of a series of measurement valuables (including the average power,  $P$ , laser repetition rate,  $\nu$ , pulse width,  $\tau$ , laser wavelength for writing,  $\lambda_{write}$ , light wavelength during the measurement,  $\lambda_{measure}$ , scan speed,  $S$ , and line spacing,  $t$ , and a material constant,  $\gamma$ , which correlates the LIRIC-induced phase change with the induced molecular density change via laser pulse energy absorption), for estimating the conversion between absorbed pulse energy and the induced phase change (Eq. (3)),

$$\Delta\phi = \gamma \cdot \frac{P^2}{\nu \cdot \tau \cdot \lambda_{write} \cdot \lambda_{measure} \cdot S \cdot t} \quad (3)$$

This new formula is now valid when the writing and reading wavelengths are different. Since our model has been shown to work well for polymer-based hydrogels [26,27], we wanted to see if it worked for cornea. Experimental data shown in the following Section 3.3 were fitted by Eq. (3) to test the validity of the model in corneal tissue. The fitted results are presented in Section 4.2. The material constant  $\gamma$  was determined from the quantitative results (Section 3.3). With the known parameter  $\gamma$  in the model, this model can then be used to predict the scaling behavior of LIRIC phase change inside transparent ophthalmic materials when laser or writing parameters are varied.

### 3. Experimental results

#### 3.1. Histological findings

Corneal tissue cross-sections were examined under 350 nm, 488 nm, and 615 nm illumination (Fig. 3). LIRIC regions were easily identified by their green autofluorescence (AF) under 488 nm illumination [34,38]. They also exhibited strong red fluorescent CHP signal under 615 nm illumination which was co-localized with the green autofluorescence signal. Examples of histological cross-sections of low and high repetition rate LIRIC writing are shown in Fig. 3.

In the case of 8.3 MHz writing and 200 mW laser power (Fig. 3(b)) severe damage occurred at the slowest scan speed of 10 mm/s. A large cavitation was seen across the corneal thickness. This was likely due to tissue disruption from the high energy deposition. A smaller degree of lamellar separation was observed in the middle of 8.3 MHz LIRIC phase bars written at 50 mm/s, and even less was seen for bars written at 100–200 mm/s. Our observations suggested weakening

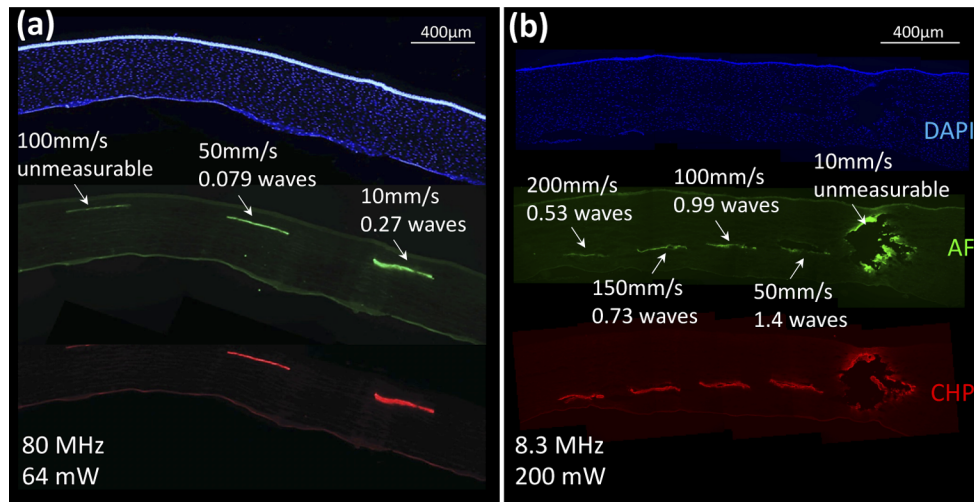


**Fig. 3.** (a) Micrographs of rabbit corneal sections (epithelium is top-most in all cases) illustrating the histological impact of Blue-LIRIC at 80 MHz and 64 mW. Blue fluorescence in the top image indicates DAPI-positive cells; green autofluorescence in the middle image denotes laser-treated areas under 488 nm illumination; red fluorescence identifies CHP-positive signals in the bottom image, which are well co-localized with the green autofluorescence signals. Single LIRIC layers were created at 3 different scan speeds from 10 mm/s to 100 mm/s, generating levels of induced phase change indicated above each bar. Note that at 100 mm/s and 80 MHz, the phase change was too low to be measured. (b) Images of rabbit corneal sections (similar orientation and staining to (a)) illustrating the histological impact of Blue-LIRIC at 8.3 MHz and 200 mW. Single LIRIC layers were created at scan speeds ranging from 10 mm/s to 200 mm/s, generating levels of induced phase change indicated above each bar. Note that at 10 mm/s, gross tissue damage occurred, and the phase change could not be measured. Unlike the 80 MHz data, there was no clear visual correlation of AF or CHP signal strength to induced phase change.

of inter-lamellar bonds, and could underlie the fractures seen with TEM (see Fig. 5 in Section 3.2 below).

Overall, these data suggest that low repetition rates and higher laser power attained higher phase change, but also resulted in disruption and potentially, localized weakening of tissue architecture.

### 3.2. Ultrastructure findings

TEM imaging of LIRIC patterns written at low power and high repetition rates showed a set of darkened tracks through the corneal stroma (Fig. 4(a)-(c)), corresponding to cross sectioning of LIRIC lines within each bar. These darkened tracks consisted of relatively parallel areas of modification of the ECM comprised of darkened collagen fibrils at the edges of an area of homogenous material (Fig. 4(d)-(e)). The lengths of the vertically oriented dark “lines” seen on the TEM images in Fig. 4 represent the axial thickness of individual LIRIC lines. In other words, Fig. 4 shows cross sections of the phase structures inscribed in a single bar, single layer pattern. The axial length of scan lines should be on the order of the Rayleigh range. But overall, it remains true that tissue processing for TEM can cause significant distortions of the material and this likely explains why the length of the lines written at 10 mm/s in Fig. 4(a) are shorter than that of the lines written at 50 mm/s in Fig. 4(b).



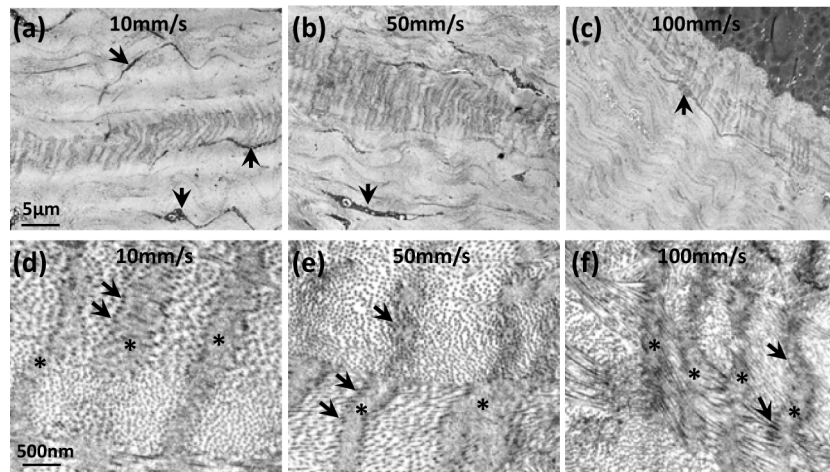


**Fig. 4.** (a) TEM micrograph of Blue-LIRIC pattern inscribed at 10 mm/s, 80 MHz and 64 mW inside the corneal stroma. Repeating areas of photo-modification can be seen as darkened tracks running roughly parallel to collagen lamellae. (b) TEM micrograph of LIRIC pattern written at 50 mm/s, 80 MHz and 64 mW. (c) TEM micrograph of LIRIC pattern written at 100 mm/s, 80 MHz and 64 mW, but which ended up close to the epithelium (dark cells at the top right of the picture). Magnification is identical for (a)-(c). Intra-stromal cells – likely keratocytes – are arrowed. (d)-(f) Higher magnification views of the LIRIC tracks in (a)-(c), illustrating their ultrastructure. At all speeds, this involved darkening of collagen fibrils around the edges (arrowed) of a vertically elongated area where the collagen fibril structure was lost, and the ECM material became relatively homogenous (\*).

Interestingly, the width of these homogenized regions scaled with the magnitude of the induced phase change and inversely with the scan speed (from 10–100 mm/s). The spacing between individual tracks was roughly  $\sim 0.5 \mu\text{m}$ , which is consistent with the line spacing of the LIRIC pattern. The fact that we could see discrete lines/tracks in the case of high repetition rate LIRIC writing may indicate that the lateral dimension of the laser-interaction region was less than half a micrometer and consistent with the calculated diffraction-limited spot size of  $0.456 \mu\text{m}$  at 80 MHz. In turn, this implies that the volume of the laser-tissue interaction region relies on the accumulated pulse fluence on a site. In the case of low pulse fluence, the grating line width was less than the line spacing, and therefore, no pulse overlap effect needed to be considered.

TEM imaging of rabbit corneas containing LIRIC patterns created at a lower repetition rate of 8.3 MHz, speeds of 100 mm/s, 150 mm/s and 200 mm/s and average power of 200 mW showed a completely different outcome compared to LIRIC patterns written at 80 MHz and 64 mW. In 8.3 MHz LIRIC, clear fractures were visible in the middle of the LIRIC patterns, running parallel to the ocular surface (Fig. 5(a)-(c)). The edges of these fractures contained a continuous zone of homogenized extracellular matrix (Fig. 5(d)) with tracks or gratings only visible at irregular intervals above or below the homogenized matrix (Fig. 5(e)). Given that the diffraction-limited spot size at 8.3 MHz was around  $0.4 \mu\text{m}$ , while the LIRIC line spacing was set to be  $0.5 \mu\text{m}$  which is close to the calculated spot size, it is not entirely surprising that individual grating lines were not seen at the center of 8.3 MHz LIRIC pattern (i.e. at the fracture site), considering spot size broadening factors like optical aberrations. As with the 80 MHz LIRIC, phase change likely only occurs in the center of the pulse where the peak power is concentrated, effectively shrinking the laser-tissue interaction zone. The high pulse fluence meant that the grating line width was wider than the line spacing. As such, the multiple pulse overlapping effect described by Eq. (2) was likely a significant factor in the observed morphology. Only at the upper and lower edges of

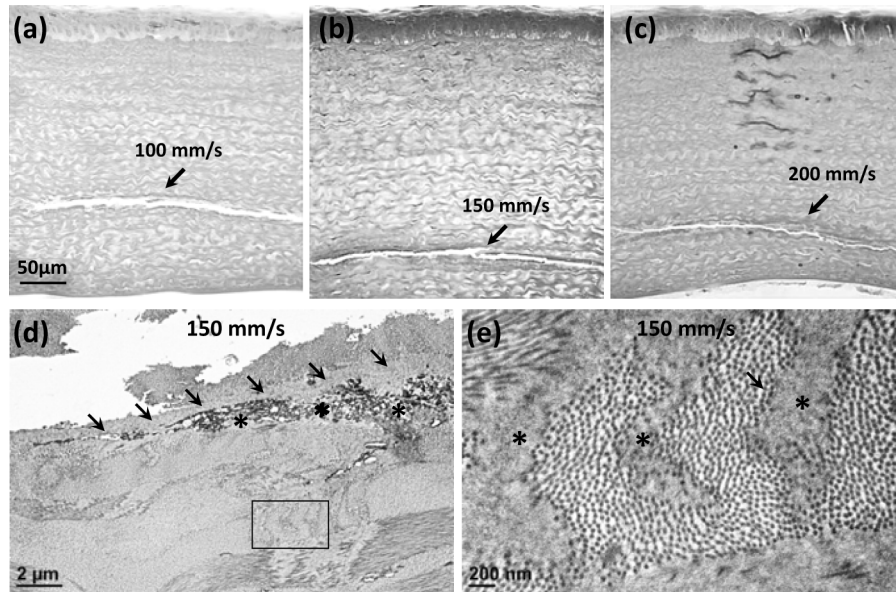


**Fig. 5.** (a)-(c) TEM micrograph of Blue-LIRIC pattern inscribed at 100 mm/s, 150 mm/s and 200 mm/s, 8.3 MHz, and 200 mW inside the corneal stroma. Clear fractures of the stromal structure can be seen in the middle of each LIRIC zone, running parallel to the collagen lamellae and the corneal surface. (d) Magnified view of part of the fracture through the LIRIC zone in the 150 mm/s pattern in (b) illustrating the continuous zone of homogenized ECM (arrowed) on the edges of the fracture, broken down cellular material likely from a dying keratocyte (\*) and the occasional tracks seen above or -in this case- below the fracture (rectangular box whose contents are further magnified in (e)). (e) Example of tracks seen periodically above or below the 8.3 MHz LIRIC patterns, which exhibited typical structure consisting of darkening of collagen fibrils around the edges (arrowed) of a vertically elongated area where the collagen fibril structure was lost and the collagenous material became relatively homogenous (\*).

each grating line, near the edge of the laser focal volume, was the power deposition sufficiently low to create distinct “lines” of tissue change. These lines were characterized by darkening of collagen fibrils at the edges and homogenization of the ECM in the middle (Fig. 5(d)-(e)). Note that the characteristics of these regions appear very similar, if not identical, to the lines or tracks observed in Fig. 4 when LIRIC patterns were inscribed at 80 MHz and 64 mW.

### 3.3. Optical phase change data

As shown in Fig. 6(a), a large amount of phase change was successfully obtained from a 1-layer LIRIC pattern at a low repetition rate with a relatively small power and a fast scan speed: for example, half a wave of phase change was attained with 110 mW and 200 mm/s at 8.3 MHz; in contrast, a much higher power (over 300 mW, system #2) was required at 80 MHz to obtain 0.5 waves of phase change. Our results suggest an enhanced efficacy at lower repetition rates compared to the same amount of phase change attained with a higher power at 80 MHz. Consequently, at a given repetition rate, the magnitude of phase change increases with power; across the three repetition rates (1, 8.3 and 80 MHz), the same amount of phase change could be obtained with a lower power by taking advantage of lower repetition rate writing. This is beneficial in terms of laser eye safety since laser energy dosage should be minimized. Another graph plotting the magnitude of phase change against the single pulse energy is shown in Fig. 6(b)

for the three repetition rates. Curiously, a larger phase change can be induced at a higher repetition rate if the single pulse energy is the same. The photochemical model in the form of Eq. (3) can be used to interpret these phenomena. At a fixed, single pulse energy, a greater number of pulses are incident on the focal plane at a higher repetition rate and thus, more pulse energy can be absorbed by the material to induce phase change; however, at a given power, the single pulse energy is greater at a lower repetition rate, which could modify the material more significantly.

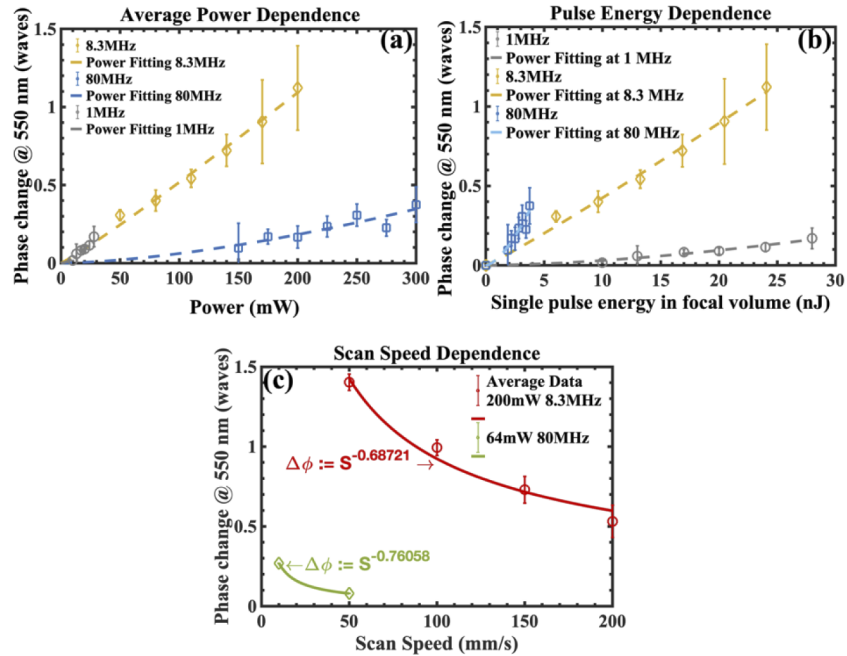


**Fig. 6.** (a) Induced phase change as a function of average power at a fixed scan speed of 200 mm/s. Quantitative experimental data were obtained at 3 repetition rates and were fitted to a power function. The exponents of the power functions are 1.63 at 1 MHz, 1.08 at 8.3 MHz and 1.57 at 80 MHz, respectively, denoting the order of multiphoton absorption process. (b) Induced phase change as a function of single pulse energy. (c) Induced phase change as a function of scan speed at a fixed power of 200 mW at 8.3 MHz and at a fixed power of 64 mW at 80 MHz. The exponents of the fitted power functions denote an inverse sub-linear relationship between the scan speed and the induced phase change.

Power functions were used to fit all the experimental data, and the power exponents were used to indicate the order of the multiphoton absorption process. The power exponents of the 1.0 and 80 MHz fitting curves were respectively found to be 1.63 and 1.57 (i.e., close to 2), suggesting a two-photon absorption process. However, the power exponent at 8.3 MHz was 1.08, which is far from the expected two-photon absorption order. This unexpectedly lower exponent could be attributed to a material saturation effect in the large signal regime, where we consider the phase change to be above 0.5 waves (for more details, see Section 4.2).

Experimental data collected by varying the scan speed from 10 mm/s to 200 mm/s are shown in Fig. 6(c), along with power function fitting. The average power was held constant at 200 mW in the case of 8.3 MHz writing and at 64 mW in the case of 80 MHz writing with system #3. The power discrepancy was due to a laser-based limitation in the 80 MHz system #3. A single LIRIC layer with measurable phase change was inscribed at 80 MHz with a scan speed of 10 mm/s. However, in order to measure phase change at 50 mm/s in the 80 MHz writing condition, above the noise floor of the MZI ( $\sim 0.1$  waves), we had to write 5 layers. The induced phase change of a

single layer written at 50 mm/s was then approximated by dividing the experimentally obtained value by a factor of 5, the number of layers, assuming that the phase shift is linear with the number of layers. Phase change induced with a higher scan speed of 100 mm/s at 80 MHz was too small to be measured, even with 5 stacked layers. Therefore, no data were recorded under this writing condition. At 8.3 MHz, severe tissue damage occurred at 10 mm/s; no quantitative data could be recorded. Quantitative data obtained from 50 mm/s to 200 mm/s showed a sub-linear, inverse scan speed dependence with an exponent close to  $-0.7$  rather than  $-1$  as predicted by the photochemical model. The exponent obtained at 80 MHz (represented by the green curve in Fig. 6(c)) was found to be  $-0.76$ , which also shows a sub-linear, inverse scan speed dependence, consistent with the one obtained at 8.3 MHz. It is noteworthy that one wave of phase change can be obtained in *ex vivo* rabbit eye globes with a single LIRIC layer, 100 mm/s and 200 mW in the case of 8.3 MHz writing, which has never been achieved before.

We also plot the induced phase change as a function of deposited total energy in the focal volume, as shown in Fig. 7. The resulting phase change increased with increased energy deposition, and a similar phase change could be obtained with a smaller total pulse energy per site by taking advantage of lower repetition rate writing. This result provides an essentially identical insight to that provided in Fig. 6(a).

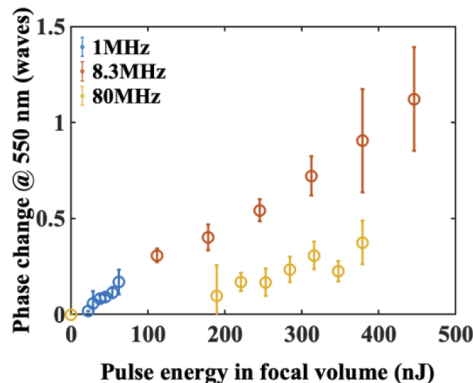


**Fig. 7.** Induced phase change as a function of the deposited pulse energy in the focal volume obtained at three repetition rates, 1 MHz, 8.3 MHz and 80 MHz.

## 4. Discussion

The present study is the first to quantify optical phase change induced in *ex vivo* rabbit corneas under a range of laser exposure conditions, and the first to correlate these LIRIC optical phase changes with biological alterations in corneal extracellular matrix organization. TEM and strong, positive CHP staining of laser-modified zones provided early insight into corneal ultrastructural, chemical, and microscopic modifications induced by LIRIC. They suggested that LIRIC disrupts collagen fibril organization and changes the molecular organization of collagen triple helices in the laser-treated area. With respect to the induced phase change, a quadratic power dependence was expected to arise from a nonlinear, two-photon absorption process, such as the one thought to dominate during LIRIC writing inside hydrogels [27,43]. Here, we found the power exponents to deviate from these expected values, suggesting that material saturation effects may be contributing significantly to the outcome.

### 4.1. Corneal tissue modifications induced by LIRIC

TEM images collected in the present study showed clear ultrastructural modifications to the regular corneal architecture that varied significantly between low and high repetition rate writing.



LIRIC at 80 MHz created a loss of normal stromal ultrastructure within each line of phase change that comprised each phase bar [see Fig. 1(a)]. Each phase line within a bar was distinctly visible because of the localized change in ultrastructure, characterized by loss of the pseudo-hexagonal arrangement of collagen fibrils and collagen D-banding [34]. The regular arrangement of collagen fibrils was replaced by a homogenous, gray area, likely containing a mixture of denatured type I and type V collagen [34,44–46]. Histological studies employing molecular probes were informative in this context and revealed the photo-modified regions to exhibit strong CHP staining, whereas the background, unmodified collagen matrix in the rest of the stroma remained CHP-negative. Although the origin of green autofluorescence in LIRIC-treated corneas is unknown, it could result from: 1) formation of fluorophores like tyrosine dimers due to photo-degradation of collagens, 2) a loss of the ultrastructure of collagen fibrils (as seen from TEM micrographs), or 3) laser-enhanced intra-collagen cross-linking [47–52]. Taken together, the co-localization of CHP binding and green autofluorescence suggests that high-repetition rate LIRIC caused – at the very least – loss of normal organization and denaturation of collagen fibrils in the laser-irradiated regions. While we can only speculate about other mechanisms, formation of tyrosine dimers remains more likely than cross-linking, especially given the finding that continuous homogenization of the collagen matrix across the entire LIRIC bars seen at 8.3 MHz led to fracturing upon tissue processing for histology and TEM. This suggests that the homogenized ECM is weaker, and less resistant to mechanical manipulation, rather than stronger, as would be expected if cross-linking was the main mechanism of action.

LIRIC patterns inscribed at 8.3 MHz also exhibited strong green auto-fluorescence and CHP staining, suggesting similar ultrastructural processes. However, these patterns caused more disruptive effects on stromal organization than 80 MHz LIRIC: individual scan lines (gratings/tracks) were no longer identifiable except at the outer edges of the patterns. Instead, both histology and TEM revealed tissue separation or fracture in the middle of the photo-modification zones at all speeds tested. The most severe of these fractures occurred with the slowest scanning speed of 10 mm/s, destroying about half of the cornea around that LIRIC bar. Higher speeds caused less disruption, but separations of the tissue were still observed. TEM analysis showed these fractures to be situated inside large, continuous zones of ECM homogenization that extended across the entire width of each LIRIC bar. As detailed earlier, we believe that these zones represent structurally weakened areas of corneal stroma that easily separate when exposed to the stresses of histological or TEM tissue processing. Wisps of short LIRIC tracks could occasionally be seen to “sprout” from these contiguous, homogenized zones, both above and below it. They exhibited the characteristic appearance of lines seen with 80 MHz LIRIC (i.e. zones of lower laser energy deposition). Clearly, additional work is needed to both understand the tissue effects observed and to establish the optimal repetition rate for performing LIRIC inside corneal tissues. Energy doses above the threshold of optical breakdown, akin to what is used in femtosecond laser refractive surgery, create large gas bubbles and cause large tissue separation. Since the goal for LIRIC is to provide optical correction while avoiding optical breakdown, optimal repetition rates will need to be carefully chosen to attain this goal. For blue laser LIRIC, the present results suggest that optimal repetition rates will fall between 8.3 and 80 MHz, with appropriate titration of laser power and scanning speed needed to generate the desired magnitude of phase change.

An important consideration for the clinical applicability of LIRIC is establishing the long-term impact of induced changes to the corneal stromal ultrastructure *in vivo*. With respect to LIRIC at 80 MHz, this has already been studied and published, showing safety and efficacy of the procedure in rabbit and cat animal models respectively, while maintaining corneal clarity and shape for 12 months post-procedure [15,17,18]. Specifically, two of those studies showed that LIRIC was able to induce close to intended Cylinder refractive change *in vivo*, a change that was maintained in the long-term [15,17]. Direct inspection, optical coherence tomography and wavefront sensing in the living eyes showed them to retain excellent optical quality, with no increase in scatter. This



was confirmed by additional experiments in hydrogels, which targeted the question of scatter induction by LIRIC patterns [16,28]. Finally, both short and medium-term longitudinal studies of 80 MHz Blue-LIRIC in rabbits and humans showed no negative impact of this procedure on corneal health [18,25]. However, with respect to 8.3 MHz LIRIC or even more “*optimized*” LIRIC at a repetition rate less than 80 MHz, the long-term consequences of induced stromal changes are not yet known. Longitudinal, *in vivo* studies will be required, although they are outside the scope of the present paper. Only if these changes are demonstrated to be safe for corneal health and if they preserve corneal clarity *in vivo* over the long term, can low-repetition rate Blue-LIRIC be considered a viable option for clinical implementation.

#### 4.2. Material saturation effects

As seen in Fig. 6, phase change increases as a function of average power and decreases with scan speed when all the other laser system parameters at each repetition rate are kept constant. The efficacy of repetition rate was assessed by comparing the amount of power required to attain the same magnitude of phase change. Lower repetition rate writing enabled a more efficient LIRIC process, with similar phase change attained with three times smaller power at 8.3 MHz compared to 80 MHz. The power dependency of the induced phase change deviated from a quadratic exponent, and the scan speed showed a sublinear inverse relationship - both unexpected from the proposed photochemical model in the form of Eq. (3).

The limitations of the photochemical model can be clearly inferred from Fig. 8(a): a large deviation between the experimental data and the photochemical model are seen in the large signal regime when the photochemical model in the form of Eq. (3) is implemented to fit the experimental data using a root least square fitting method.

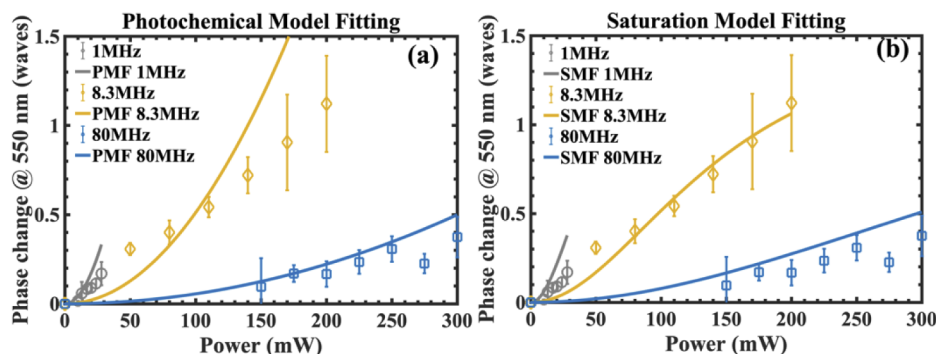


**Fig. 8.** (a) Quantitative experimental data were fitted by the photochemical model fitting (PMF). Deviation between the experimental data and the model is noticeable at large signal regimes. (b) The modified photochemical model with a saturation factor, represented as a saturation model fitting (SMF), is applied to fit data, and yields a good agreement.

We posit that the discrepancy between the experimental data and the photochemical model can be attributed to the material saturation at large phase changes, which may result from a fixed number of molecules available for modification. Additionally, the material saturation effect might arise from the incubation effect which associates the nonlinear absorption coefficient with the number of pulses on the same site [53,54]. The linear accumulation assumption might not be accurate enough as the material might have been changed by the incidence of earlier pulses. Therefore, a phenomenological saturation factor in analogy with saturation of an absorber or a gain medium is incorporated into the photochemical model from a macroscopic point of view

[55],

$$\Delta\phi = \frac{\phi_0}{1 + \frac{\phi_0}{\phi_s}} \quad (4)$$

where  $\phi_0$  is the induced phase change in the small signal regime as expressed in Eq. (3), and  $\phi_s$  is the saturable phase change, a material constant that depends on the interaction volume and needs to be determined. After applying the saturation model in the form of Eq. (4) to fit the data, the saturable phase change was found to be  $\sim 1.64$  waves. In the case of the original photochemical model (as shown in Eq. (3)), the material constant  $\gamma$  was  $1.8 \times 10^{-24}$  waves $\cdot$ m<sup>4</sup> / (W<sup>2</sup>  $\cdot$ s) after fitting the data at 8.3 MHz; in the case of the modified photochemical model including a saturation factor,  $\gamma$  was determined to be  $2.65 \times 10^{-24}$  waves $\cdot$ m<sup>4</sup> / (W<sup>2</sup>  $\cdot$ s) after fitting the data at 8.3 MHz as well. Table 2 lists the material constants and saturation phase change determined from both the photochemical model and the saturation model. Material constants in two cases were kept the same to fit data obtained at two other repetition rates. The modified photochemical model was in a good agreement with the experimental data as shown in Fig. 8(b), verifying that the saturation model was more reliable to reproduce the experimental data. One could see that there was a significant improvement for all 7 data obtained at 8.3 MHz after adding the saturation factor. The saturation effect was most significant in the large signal region ( $>0.5$  waves). At 80 MHz and 1 MHz, the maximum induced phase changes were pretty small, less than 0.5 waves, due to the limited maximum power output of the laser. Therefore, for these two repetition rates, there was no significant saturation effect at the range of powers tested presently. Consequently, it was no surprise to see no substantial improvement of the saturation model over the photochemical model for these two repetition rates (compare Fig. 8(a) and Fig. 8(b) fits). Due to the presence of material saturation, the induced phase change cannot increase indefinitely, and the growth rate of the phase change would vanish gradually, manifesting as the deviation from the originally expected growth trend. This photochemical model with saturation, although simple, also worked well on the data collected from hydrogel-based contact lenses [27].

**Table 2. Fitted material constant  $\gamma$  and saturation phase change  $\Phi_s$**

	Fitted Repetition Rate (MHz)	Material Constant $\gamma$ (waves $\cdot$ m <sup>4</sup> / (W <sup>2</sup> $\cdot$ s))		Maximum Achievable RI change	Saturation Phase Change $\Phi_s$ (waves) in SMF	$R^2$	
		PMF	SMF			PMF	SMF
Power Scaling Experiment	8.3	$1.8 \times 10^{-24}$	$2.65 \times 10^{-24}$	0.031	1.64	0.73	0.96
Scan Speed Scaling Experiment	8.3	$3.5 \times 10^{-25}$	$6.4 \times 10^{-25}$	0.039	2.74	0.69	0.99

The effect of a saturation factor can also be verified by fitting the results from scan speed scaling experiments (Fig. 6(c)) with the saturation model. As shown in Fig. 9, the averaged data (shown by red circles) obtained at 8.3 MHz can be fitted well by the modified photochemical model with a saturation factor and the coefficient of determination  $R^2$  value increased from 0.69 to 0.99 after the saturation model fitting, signifying a good agreement. The saturable phase change,  $\phi_s$ , determined from the scan speed scaling experiment was  $\sim 2.74$  waves and the material constant,  $\gamma$ , was found to be  $6.4 \times 10^{-25}$  waves $\cdot$ m<sup>4</sup> / (W<sup>2</sup>  $\cdot$ s). Differences can be found between the numbers obtained from the scan speed scaling experiment and those from the power scaling experiment, which could be caused by the imperfect qualities of biological tissues and discrepancies among multiple trials. This result renders the modified saturation model a promising approach to performing data interpretation and predicting the scaling behavior of induced phase change under various laser exposure conditions.

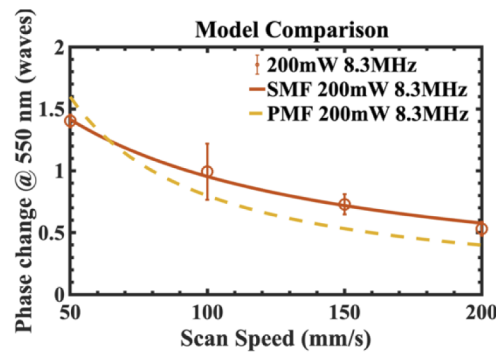


**Fig. 9.** Both the photochemical model fitting (PMF) and the saturation model fitting (SMF) were used to fit the experimental data at 8.3 MHz. The saturation model yields a higher coefficient of determination  $R^2$ , manifesting itself as a more reliable way to describe the scaling behavior of the induced phase change inside corneal tissues.

#### 4.3. Conclusions and future work

Phase bars were inscribed with Blue-LIRIC into the mid-stromal region of *ex vivo* rabbit corneas to examine the influence of different repetition rates, scan speeds, and laser power both on tissue structural changes and how they related to the magnitude of induced optical phase change. The use of low-repetition-rate femtosecond laser pulses dramatically enhanced the efficacy of LIRIC, generating a very large amount of phase change at a lower power and with a faster scan speed. This result is promising in terms of the clinical applications of LIRIC. Importantly, our experimental data were well fitted by a modified photochemical model incorporating a material saturation factor. This model was designed to work for any transparent materials that could elicit an optical phase change upon exposure to ultrashort laser pulses via a multi-photon-absorption process. We propose that this modified model may be a useful new tool for predicting the scaling behavior of induced phase change under different laser exposure conditions. This new tool will be instrumental in future work that aims to better understand the factors contributing to the chemical and ultrastructural changes, which underlie LIRIC's measured phase changes.

**Funding.** National Eye Institute (P30 EY001319); Clerio Vision inc. (005735, 058149-002); Empire State Development's Division of Science, Technology and Innovation (005420); National Science Foundation (IIP: 1549700); Center for Emerging and Innovative Sciences (C090130, C150130).

**Acknowledgements.** The authors thank Margaret DeMagistris and Thurma McDaniel for their technical support with tissue processing, corneal sectioning, tissue staining and photo-microscopy. Portions of this work were presented at SPIE Photonics West 2020, "Enhanced Efficacy in Refractive Index Modifications of Rabbit Eye Globe *ex-vivo* with Low Repetition Rate Blue Femtosecond Laser Pulses".

**Disclosures.** WHK has founder's equity in Clerio Vision, and he is Chief Science Officer, but has no fiduciary or management responsibility. KRH has founder's equity in Clerio Vision Inc., but no fiduciary responsibility. LZ is an employee of, and has equity in Clerio Vision Inc.

**Data availability.** Data underlying the results presented in this paper are available here: Ref. [56].

#### References

1. L. Y. Chen and E. E. Manche, "Comparison of femtosecond and excimer laser platforms available for corneal refractive surgery," *Curr. Opin. Ophthalmol.* **27**(4), 316–322 (2016).
2. Z. S. Bashir, M. H. Ali, A. Anwar, M. H. Ayub, and N. H. Butt, "Femto-LASIK: the recent innovation in laser assisted refractive surgery," *J. Pak. Med. Assoc.* **67**, 609 (2017).
3. S. H. Chung and E. Mazur, "Surgical applications of femtosecond lasers," *J. Biophotonics* **2**(10), 557–572 (2009).
4. R. Krueger, S. Trokel, and H. Schubert, "Interaction of ultraviolet laser light with the cornea," *Invest. Ophthalmol. Vis. Sci.* **26**, 1455–1464 (1985).
5. R. Ambrósio Jr, T. Tervo, and S. E. Wilson, "LASIK-associated dry eye and neurotrophic epitheliopathy: pathophysiology and strategies for prevention and treatment," *J. Refract. Surg.* **24**(4), 396–407 (2008).

6. K. Nakamura, D. Kurosaka, H. Bissen-Miyajima, and K. Tsubota, "Intact corneal epithelium is essential for the prevention of stromal haze after laser assisted in situ keratomileusis," *Br. J. Ophthalmol.* **85**(2), 209–213 (2001).
7. F. H. de Paula, C. G. Khairallah, L. M. Niziol, D. C. Musch, and R. M. Shtein, "Diffuse lamellar keratitis after laser in situ keratomileusis with femtosecond laser flap creation," *J. Cataract. Refract. Surg.* **38**(6), 1014–1019 (2012).
8. M. V. Netto, R. R. Mohan, R. Ambrósio Jr, A. E. Hutcheon, J. D. Zieske, and S. E. Wilson, "Wound healing in the cornea: a review of refractive surgery complications and new prospects for therapy," *Cornea* **24**(5), 509–522 (2005).
9. G. Yoon, S. MacRae, D. R. Williams, and I. G. Cox, "Causes of spherical aberration induced by laser refractive surgery," *J. Cataract. Refract. Surg.* **31**(1), 127–135 (2005).
10. P. S. M. D. Binder, "Analysis of ectasia after laser in situ keratomileusis: risk factors," *J. Cataract. Refract. Surg.* **33**(9), 1530–1538 (2007).
11. S. Marcos, S. Barbero, L. Llorente, and J. Merayo-Llodes, "Optical response to LASIK surgery for myopia from total and corneal aberration measurements," *Invest. Ophthalmol. Vis. Sci.* **42**, 3349–3356 (2001).
12. M. R. Santhiago, N. T. Giacomini, D. Smadja, and S. J. Bechara, "Ectasia risk factors in refractive surgery," *OPHTH* **10**, 713–720 (2016).
13. K. T. Wozniak, S. M. Gearhart, D. E. Savage, J. D. Ellis, W. H. Knox, and K. R. Huxlin, "Comparable change in stromal refractive index of cat and human corneas following blue-IRIS," *J. Biomed. Opt.* **22**(5), 055007 (2017).
14. L. Xu, W. H. Knox, M. DeMagistris, N. Wang, and K. R. Huxlin, "Noninvasive intratissue refractive index shaping (IRIS) of the cornea with blue femtosecond laser light," *Invest. Ophthalmol. Vis. Sci.* **52**(11), 8148–8155 (2011).
15. D. E. Savage, D. R. Brooks, M. DeMagistris, L. Xu, S. MacRae, J. D. Ellis, W. H. Knox, and K. R. Huxlin, "First demonstration of ocular refractive change using blue-IRIS in live cats," *Invest. Ophthalmol. Vis. Sci.* **55**(7), 4603–4612 (2014).
16. G. A. Gandara-Montano, L. Zheleznyak, and W. H. Knox, "Optical quality of hydrogel ophthalmic devices created with femtosecond laser induced refractive index modification," *Opt. Mater. Express* **8**(2), 295–313 (2018).
17. D. R. Brooks, K. T. Wozniak, W. Knox, J. D. Ellis, and K. R. Huxlin, "Measurement and design of refractive corrections using ultrafast laser-induced intra-tissue refractive index shaping in live cats," in *Ophthalmic Technologies XXVIII* (International Society for Optics and Photonics, 2018), p. 104741B.
18. K. T. Wozniak, S. C. Butler, X. He, J. D. Ellis, W. H. Knox, and K. R. Huxlin, "Temporal evolution of the biological response to laser-induced refractive index change (LIRIC) in rabbit corneas," *Exp. Eye Res.* **207**, 108579 (2021).
19. L. Ding, W. H. Knox, J. Bühren, L. J. Nagy, and K. R. Huxlin, "Intratissue refractive index shaping (IRIS) of the cornea and lens using a low-pulse-energy femtosecond laser oscillator," *Invest. Ophthalmol. Vis. Sci.* **49**(12), 5332–5339 (2008).
20. L. J. Nagy, L. Ding, L. Xu, W. H. Knox, and K. R. Huxlin, "Potentiation of femtosecond laser intratissue refractive index shaping (IRIS) in the living cornea with sodium fluorescein," *Invest. Ophthalmol. Vis. Sci.* **51**(2), 850–856 (2010).
21. D. Brooks, "Design of intra-tissue refractive index shaping systems and their implementation in creating refractive structures in live cats," (2018).
22. L. Xu, W. H. Knox, and K. R. Huxlin, "Exogenous and endogenous two-photon absorption for intra-tissue refractive index shaping (IRIS) in live corneal tissue [Invited]," *Opt. Mater. Express* **1**(7), 1159 (2011).
23. G. A. Gandara-Montano, A. Ivansky, D. E. Savage, J. D. Ellis, and W. H. Knox, "Femtosecond laser writing of freeform gradient index microlenses in hydrogel-based contact lenses," *Opt. Mater. Express* **5**(10), 2257–2271 (2015).
24. S. C. Butler, C. Leeson, K. R. Huxlin, J. D. Ellis, W. Knox, I. G. Cox, G. Yoon, S. M. MacRae, and L. Zheleznyak, "Next generation diffractive multifocal contact lenses for presbyopia correction using LIRIC," *Invest. Ophthalmol. Vis. Sci.* **60**, 3723 (2019).
25. L. Zheleznyak, S. C. Butler, I. G. Cox, K. R. Huxlin, J. D. Ellis, W. Knox, K. Waltz, J. A. Vukich, G. Quesada, R. Quesada, A. Melendez, J. J. Machat, and S. M. MacRae, "First-in-human laser-induced refractive index change (LIRIC) treatment of the cornea," *Invest. Ophthalmol. Visual Sci.* **60**, 5079 (2019).
26. R. Huang and W. H. Knox, "Quantitative photochemical scaling model for femtosecond laser micromachining of ophthalmic hydrogel polymers: effect of repetition rate and laser power in the four photon absorption limit," *Opt. Mater. Express* **9**(3), 1049–1061 (2019).
27. R. Huang and W. H. Knox, "Femtosecond micro-machining of hydrogels: parametric study and photochemical model including material saturation," *Opt. Mater. Express* **9**(9), 3818–3834 (2019).
28. K. T. Wozniak, T. A. Germer, S. C. Butler, D. R. Brooks, K. R. Huxlin, and J. D. Ellis, "Scattering properties of ultrafast laser-induced refractive index shaping lenticular structures in hydrogels," in *Frontiers in Ultrafast Optics: Biomedical, Scientific, and Industrial Applications XVIII* (International Society for Optics and Photonics 2018), p. 1052205.
29. D. Li, D. Jani, J. Linhardt, J. F. KÜnzler, S. Pawar, G. Labenski, T. Smith, and W. H. Knox, "Optimization of femtosecond laser micromachining in hydrogel polymers," *J. Opt. Soc. Am. B* **26**(9), 1679–1687 (2009).
30. D. Li, L. Gustavo Cancado, L. Novotny, W. H. Knox, N. Andersen, D. Jani, J. Linhardt, R. I. Blackwell, and J. F. KÜnzler, "Micro-Raman spectroscopy of refractive index microstructures in silicone-based hydrogel polymers created by high-repetition-rate femtosecond laser micromachining," *J. Opt. Soc. Am. B* **26**(4), 595–602 (2009).
31. D. Yu, R. Huang, and W. H. Knox, "Femtosecond laser micromachining in ophthalmic hydrogels: spectroscopic study of materials effects," *Opt. Mater. Express* **9**(8), 3292–3305 (2019).

32. D. Yu, E. B. Brown, K. R. Huxlin, and W. H. Knox, "Tissue effects of intra-tissue refractive index shaping (IRIS): insights from two-photon autofluorescence and second harmonic generation microscopy," *Biomed. Opt. Express* **10**(2), 855–867 (2019).
33. A. Vogel, N. Linz, S. Freidank, and G. Paltauf, "Femtosecond-laser-induced nanocavitation in water: implications for optical breakdown threshold and cell surgery," *Phys Rev Lett* **100**(3), 038102 (2008).
34. D. E. Savage, *A non-ablative technique for femtosecond laser-based refractive correction: development, efficacy, and tissue effects* (University of Rochester, 2018).
35. G. A. Gandara-Montano, V. Stoy, M. Dudič, V. Petrák, K. Haškovcová, and W. H. Knox, "Large optical phase shifts in hydrogels written with femtosecond laser pulses: elucidating the role of localized water concentration changes," *Opt. Mater. Express* **7**(9), 3162–3180 (2017).
36. M. Takeda, H. Ina, and S. Kobayashi, "Fourier-transform method of fringe-pattern analysis for computer-based topography and interferometry," *J. Opt. Soc. Am.* **72**(1), 156 (1982).
37. M. Takeda, "Spatial-carrier fringe-pattern analysis and its applications to precision interferometry and profilometry: an overview," *Industrial Metrology* **1**(2), 79–99 (1990).
38. K. T. Wozniak, N. Elkins, D. R. Brooks, D. E. Savage, S. MacRae, J. D. Ellis, W. H. Knox, and K. R. Huxlin, "Contrasting cellular damage after Blue-IRIS and Femto-LASIK in cat cornea," *Exp. Eye Res.* **165**, 20–28 (2017).
39. J. Kapuscinski, "DAPI: a DNA-specific fluorescent probe," *Biotech. Histochem.* **70**(5), 220–233 (1995).
40. J. L. Zitnay, Y. Li, Z. Qin, B. H. San, B. Depalle, S. P. Reese, M. J. Buehler, S. M. Yu, and J. A. Weiss, "Molecular level detection and localization of mechanical damage in collagen enabled by collagen hybridizing peptides," *Nat. Commun.* **8**(1), 14913–12 (2017).
41. Y. Li, C. A. Foss, D. D. Summerfield, J. J. Doyle, C. M. Torok, H. C. Dietz, M. G. Pomper, and S. M. Yu, "Targeting collagen strands by photo-triggered triple-helix hybridization," *Proc. Natl. Acad. Sci.* **109**(37), 14767–14772 (2012).
42. R. Huang, D. Yu, and W. H. Knox, "Enhanced efficacy in refractive corrections of rabbit corneas with low repetition rate blue femtosecond laser pulses," in *Frontiers in Ultrafast Optics: Biomedical, Scientific, and Industrial Applications XX* (International Society for Optics and Photonics, 2020), p. 112700Q.
43. R. Huang and W. H. Knox, "Femtosecond Micromachining of Ophthalmic Hydrogels: effects of laser repetition rate on the induced phase change in the two photon and four photon absorption limit," in *CLEO: Applications and Technology* (Optical Society of America, 2019), p. AW4I. 5.
44. T. F. Linsenmayer, J. M. Fitch, T. M. Schmid, N. Zak, E. Gibney, R. D. Sanderson, and R. Mayne, "Monoclonal antibodies against chicken type V collagen: production, specificity, and use for immunocytochemical localization in embryonic cornea and other organs," *J. Cell Biol.* **96**(1), 124–132 (1983).
45. J. M. Fitch, J. Gross, R. Mayne, B. Johnson-Wint, and T. F. Linsenmayer, "Organization of collagen types I and V in the embryonic chicken cornea: monoclonal antibody studies," *Proc. Natl. Acad. Sci.* **81**(9), 2791–2795 (1984).
46. J. M. Fitch, D. E. Birk, A. Mentzer, K. A. Hasty, C. Mainardi, and T. F. Linsenmayer, "Corneal collagen fibrils: dissection with specific collagenases and monoclonal antibodies," *Invest. Ophthalmol. Vis. Sci.* **29**, 1125–1136 (1988).
47. M. J. Davies and R. J. Truscott, "Photo-oxidation of proteins and its role in cataractogenesis," *J. Photochem. Photobiol. B: Biol.* **63**(1-3), 114–125 (2001).
48. K. M. Bottós, C. V. Regatieri, J. L. Dreyfuss, A. A. Lima-Filho, H. B. Nader, P. Schor, and W. Chamon, "Immunofluorescence confocal microscopy of porcine corneas following collagen cross-linking treatment with riboflavin and ultraviolet A," *J. Refract. Surg.* **24**(7), S715–S719 (2008).
49. V. Hovhannisyan, W. Lo, C. Hu, S.-J. Chen, and C. Y. Dong, "Dynamics of femtosecond laser photo-modification of collagen fibers," *Opt. Express* **16**(11), 7958–7968 (2008).
50. V. Hovhannisyan, A. Ghazaryan, Y.-F. Chen, S.-J. Chen, and C.-Y. Dong, "Photophysical mechanisms of collagen modification by 80 MHz femtosecond laser," *Opt. Express* **18**(23), 24037–24047 (2010).
51. A. Manickavasagam, L. Hirvonen, L. Melita, E. Chong, R. Cook, L. Bozec, and F. Festy, "Multimodal optical characterisation of collagen photodegradation by femtosecond infrared laser ablation," *Analyst* **139**(23), 6135–6143 (2014).
52. C. Wang, M. Fomovsky, G. Miao, M. Zyablitskaya, and S. Vukelic, "Femtosecond laser crosslinking of the cornea for non-invasive vision correction," *Nat. Photonics* **12**(7), 416–422 (2018).
53. A. Rosenfeld, M. Lorenz, R. Stoian, and D. Ashkenasi, "Ultrashort-laser-pulse damage threshold of transparent materials and the role of incubation," *Appl. Phys. A* **69**(7), S373–S376 (1999).
54. D. Ashkenasi, A. Rosenfeld, and R. Stoian, "Laser-induced incubation in transparent materials and possible consequences for surface and bulk micro-structuring with ultrashort pulses," in *Commercial and Biomedical Applications of Ultrafast and Free-Electron Lasers* (International Society for Optics and Photonics, 2002), pp. 90–98.
55. M. Hercher, "An analysis of saturable absorbers," *Appl. Opt.* **6**(5), 947–954 (1967).
56. R. Huang, D. Yu, D. Savage, K. Wozniak, L. Zheleznyak, K. Huxlin, and W. Knox, "Dataset," figshare, 2021, <https://doi.org/10.6084/m9.figshare.16958272.v1>.